

# Three-Dimensional Full-Wave Transient Analysis of Switches and Faults using a Method of Moments Solution of the Electric Field Integral Equation

Mohammad Shafieipour, Jeewantha De Silva, Moein Nazari, Simon Fortin, Farid Paul Dawalibi

**Abstract**—Three-dimensional full-wave electromagnetic transient (EMT) analysis of switches and faults is shown to be possible in the time domain (TD) from numerical solutions of Maxwell’s equations in the frequency domain (FD). The electric field integral equation is solved by the method of moments for the initial fault or switch condition (open/closed). The problem is then cast into subsequent FD problems based on the principle of superposition. At each stage, the FD solution is converted into TD and modified by appropriate functions selected to enforce the desired switch operation (closing/opening) in the next stage. This is also applicable to applying and clearing faults at desired times. In order to navigate between the TD and FD solutions, the fast Fourier transforms are applied and a systematic procedure for obtaining a numerically convergent solution is introduced. For slow transients, results exhibit excellent agreement with simulations obtained from an EMT-type program. However, when faster transients are considered (e.g. in gas-insulated substations), the proposed method is shown to provide more realistic results than those computed by the conventional EMT simulations.

**Keywords:** Three-dimensional electromagnetic transient (3-D EMT) analysis, method of moments (MoM), electric field integral equation (EFIE), breaker, switch, fault, superposition principle.

## I. INTRODUCTION

ELECTROMAGNETIC transient (EMT) analysis is an important part of today’s design and optimization of electric power systems. While EMT is inherently represented in time domain (TD), frequency dependence is an essential characteristic of electric power systems and associated equipment. Therefore, methods based on both TD and frequency domain (FD) have been used for EMT analysis using both circuit-theory [1], [2] and field-theory [3], [4] approaches. Methods based on circuit theory are fast and convenient as they can be applied to many engineering problems with already-established general-purpose solvers such as EMT-type programs [1]. However, simplifications made in circuit-theory-based techniques such as the transverse electromagnetic (TEM) assumptions, may impose limitations on their applicability to certain engineering problems [1], [3], [5]–[7]. **For example, typical EMT commercial solvers do not consider complex configurations and situations such as non-**

**parallel lines, multilayer earth, frequency dependent soil parameters, electromagnetic field distortions at the terminals of short lines, non-conventional cable geometries, detailed and realistic cable configurations and bonding to three-dimensional (3-D) grounding systems buried in complex soil structures (not to a lumped ground impedance) which is required for accurate and critical safety-related computation results at the surface of the soil. Furthermore, the classical transmission line equations are validated up to 1 MHz [8] and are known to neglect high-frequency phenomena unless extended to high-frequency formulations [7]. Therefore, it becomes imperative to validate circuit-based models before they can be used in real-life applications. One way to achieve this, is to compare simulation results with measurement results and use the verified model for further analysis. However, measurement results are difficult to setup and interpret and are not always available, especially when designing new systems. Therefore, the full-wave 3-D modeling of power systems based on field theory has gained interest in recent years, as it is feasible to obtain such simulations with today’s typical personal computers. This is sometimes referred to as “numerical electromagnetic analysis” [1], [5] and has been used either as the primary modeling tool or as a means to validate circuit-based models. It is performed using computational electromagnetic techniques [6] such as the finite difference time domain (FDTD) method [3], [9] or the method of moments (MoM) [4], [10]. Generally, FDTD is known for its applicability to a wide range of applications. However, it can quickly become a computationally expensive task when problem size increases. This is due to the fact that FDTD discretizes the entire space and time as it solves the differential form of Maxwell’s equations directly in TD. Therefore, acceleration techniques such as the use of graphics processing units have been suggested when modeling practical examples of power systems using the FDTD [9]. In contrast, MoM is widely used for solving the integral form of Maxwell’s equations in FD which allows for limiting the discretization of geometry to its boundaries via surface integral equations such as the electric field integral equation (EFIE). Moreover, FDTD requires truncating the 3-D domain using absorbing boundary conditions or perfect matching layers in order to emulate reflection-free radiation. On the contrary, MoM can compute the electromagnetic fields everywhere in the problem domain through the dyadic Green’s functions [4]. Another advantage of solving integral equations especially for large-scale problems is that the Green’s function propagates electromagnetic fields from one location to another accurately. Hence, no grid dispersion errors exist which are**

M. Shafieipour, M. Nazari, S. Fortin, and F. P. Dawalibi are with Safe Engineering Services & technologies ltd., Laval, QC H7L6E8, Canada (e-mail: Mohammad.Shafieipour@sestech.com, Moein.Nazari@sestech.com, Simon.Fortin@sestech.com, Farid.Dawalibi@sestech.com)

J. De Silva is with Manitoba Hydro International Ltd., Winnipeg, Canada (e-mail: jeewantha@mhi.ca)

Paper submitted to the International Conference on Power Systems Transients (IPST2021) in Belo Horizonte, Brazil June 6-10, 2021.

typical to numerical differential equation solvers, which also suffer consequently from cumulative phase errors of the wave velocity. Of course, one can use a finer mesh or higher order basis functions at the expense of significant increase of computation time. Therefore, despite its FD nature, MoM is an attractive candidate for full-wave 3-D EMT analysis by computing the results in FD and transforming them into TD using efficient TD-FD interfacing techniques [11] such as the fast Fourier transform (FFT). This has been extensively used for full-wave 3-D modeling of lightning transients [4]. However, MoM cannot directly model intrinsically time-dependent operations such as opening and closing of switches or applying and clearing faults which are essential in many EMT studies.

In this paper, we show that it is indeed possible to perform a full-wave 3-D EMT analysis of switch operations and faults by solving the EFIE. For that purpose, we adopt a commercial MoM implementation specifically designed for power systems [12]. It can be used for full-wave 3-D modeling of power system equipment such as transmission lines, transformers, coaxial and pipe-type cables, towers, metallic surfaces and enclosures, etc., in the presence of frequency-dependent uniform or multilayer soil over frequencies ranging from DC to several GHz. It is shown that similarly to the technique used for performing switch operations in circuit-based FD methods (see for example [2] and the references therein), the principle of superposition can be applied for full-wave modeling of switching transients using MoM and FFT. Furthermore, a systematic procedure is introduced for ensuring accurate 3-D EMT results while minimizing the number of MoM runs, thereby optimizing the computational efficiency. The methodology is verified against simulation results obtained from an EMT-type software [13]. It should be noted that in the context of circuit-based FD techniques, it is sometimes recommended to apply the numerical Laplace transform (NLT) [2] and logarithmic FD partitioning [14] to obtain EMT results. However, in this paper we focus on the use of the standard (uniform) FFT and we investigate such modifications in future work. Furthermore, the discussion in this paper is limited to switches and faults while nonlinear devices are left for future studies.

## II. THE PROPOSED METHODOLOGY

### A. Elementary switches

Consider a general switching device (e.g., a breaker) shown in Fig. 1 placed in an arbitrary network. Let us first assume for simplicity, that this switch can only operate once at an arbitrary time  $t_s > 0$ . That is, it can only open or close but not open and/or close multiple times. Based on such simplifications, two independent devices can be defined as follows. 1) A device that is open at its initial TD stage ( $0 \leq t \leq t_s$ ) but can be closed at  $t_s$  and remain in this final stage ( $t > t_s$ ). We call this device a ‘‘closer’’. 2) A device that is closed at its initial TD stage ( $0 \leq t \leq t_s$ ) but can be opened at  $t_s$  and remain in this final stage ( $t > t_s$ ). We call this device an ‘‘opener’’.



Fig. 1. A general switch in an arbitrary network.

The above definitions are illustrated in Fig. 2 where the key characteristics of such devices are shown. In particular, the voltage across a closer at its initial TD stage can be obtained by assuming that it is an open circuit (gap), while its voltage at its final TD stage is known to be zero. Similarly, the current going through an opener at its initial TD stage can be obtained by assuming that it is a short circuit (short) while its current at its final TD stage is known to be zero. As seen in Section II-E, such elementary devices facilitate general switch operations.

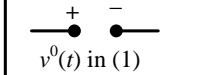
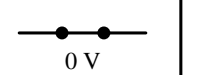
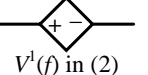
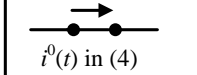
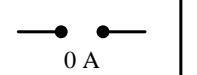
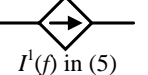
	Initial TD stage ( $0 \leq t \leq t_s$ )	Final TD stage ( $t > t_s$ )	FD equivalent for both TD stages
Closer voltage			
Opener current			

Fig. 2. Voltage of a closer and current in an opener at different TD stages.

### B. MoM excitation for a closer

In order to obtain the MoM excitation for a closer, a gap is first placed instead of the switch in the network and the voltage across it is computed in FD using MoM and then converted to TD. Depending on the FD components of the network’s energization, a single or multiple MoM runs are required to obtain such TD signal. In certain applications such as lightning studies [4], the network is excited with a lightning surge containing multiple FD components which are typically obtained by applying the FFT on the TD surge signal. Thus, multiple MoM runs in conjunction with the inverse FFT (IFFT) are necessary to compute the required TD results. However, for studies involving switch operations and fault analysis, the network is typically energized at the fundamental frequency (50 or 60 Hz) using one or multiple voltage sources to represent electric generation sites. It is also possible to apply a DC source (0 Hz), particularly when performing short and open circuit tests [6]. Therefore, in this paper, we limit the network energization(s) to a single frequency (i.e., 0, 50, or 60 Hz) for which a single MoM run is sufficient. The computed gap voltage is represented in TD as

$$v^0(t) = \begin{cases} A_v, & f = 0 \\ A_v \cdot \sin(2\pi ft + \varphi_v), & f > 0 \end{cases} \quad (1)$$

where  $A_v$  and  $\varphi_v$  are the magnitude and phase of the voltage difference across the gap produced by MoM with  $f$  being the source frequency. Note that in (1) and throughout the paper, a superscript  $k$  indicates that a parameter corresponds to the  $k^{\text{th}}$  switch operation, with 0 referring to the initial or final TD stages shown in Fig. 2. From (1), the voltage at the initial stage of a closer is obtained in TD. In order to enforce both initial and final stages of the closer in FD, the switch is replaced by a voltage source in MoM with an excitation that enforces both initial and final TD stages of Fig. 2 in FD

$$V^1(f) = FFT\{\sigma_1(t, t_r) \cdot v^0(t) \cdot \sigma_2(t, t_s)\} \quad (2)$$

where  $v^0(t)$  is defined in (1) and

$$\sigma_1(t, t_r) = \begin{cases} t/t_r, & 0 \leq t < t_r \\ 1, & t \geq t_r \end{cases}, \sigma_2(t, t_s) = \begin{cases} 1, & 0 \leq t \leq t_s \\ 0, & t > t_s \end{cases}. \quad (3)$$

In (2) and (3),  $t_r$  is the ramp-up time. While  $\sigma_1(t, t_r)$  is not required by the conditions in Fig. 2, it is included in (2) to ensure causality. In EMT-type programs,  $t_r$  is typically chosen to be an integer number of source cycles to improve numerical stability (i.e.,  $t_r = q/f, q \in \mathbb{N}$ ) [13]. In (2), inclusion of  $t_r$  makes the expression inside the curly brackets uniquely representable by a periodic function. This improves the accuracy of computations in a way that can be explained using Fig. 5 (Section III). It consists of a TD vs. FD representation of a typical excitation based on (1) and (2) at 50 Hz. In the TD plot,  $\sigma_1 \cdot v^0 \cdot \sigma_2$  is influenced by  $\sigma_1$  from 0 to  $t_r = 0.02$  s and is abruptly set to zero after  $t_s = 0.03$  s as it is multiplied by  $\sigma_2$ . As seen in the FD plot of Fig. 5, the spectrum of such a signal (i.e., a signal that starts and ends at zero magnitude) steadily decreases as the frequency increases, with negligible oscillations. This makes it less prone to truncation errors in FD and thus well-suited for FFT/IFFT operations. It is worth noting that (2) is similar to (23) in [2] but with modifications that facilitates its application to MoM and the FFT as a standard and efficient interfacing technique between TD and FD [11]. As exemplified in Fig. 5,  $V^1(f)$  in (2) cannot be represented by a single frequency and multiple MoM runs are required for such excitations. In Section II-D, a systematic procedure is introduced for selecting an efficient set of discrete frequencies when applying MoM switch excitations.

### C. MoM excitation for an opener

The steps for deriving the excitation of an opener are similar to those for a closer, with the gap replaced by a short and with the voltage source replaced by a current source, according to Fig. 2. That is, the current flowing in the short in its initial TD stage is

$$i^0(t) = \begin{cases} A_i, & f = 0 \\ A_i \cdot \sin(2\pi ft + \varphi_i), & f > 0 \end{cases} \quad (4)$$

where  $A_i$  and  $\varphi_i$  are the magnitude and phase of the current going through the short as computed by the MoM. Subsequently, both initial and final TD stages of the opener in FD are imposed by replacing the switch with a current source and applying the excitation according to Fig. 2 as follows

$$I^1(f) = \text{FFT}\{\sigma_1(t, t_r) \cdot i^0(t) \cdot \sigma_2(t, t_s)\} \quad (5)$$

where  $i^0(t)$  and  $\sigma_{1,2}(t, x)$  are defined in (4) and (3), respectively. Again, this is similar to (24) of [2] but more suited for MoM and FFT. When opening a switch, it is customary to assume  $t_s$  to be the first zero-crossing of the current signal after the time the switch (i.e., a breaker) is opened [2], [13]. However, this is not required by the superposition principle but is rather user dependent. In fact, as exemplified in Fig. 7, a switch is opened at the time a fault is cleared, not at the next zero crossing of the current waveform.

### D. Superposition principle for MoM switch excitations

The superposition principle is used to perform switch operations using MoM. This requires solving the MoM system at different frequencies based on the applied excitation. In this section, a systematic procedure for such simulations is

proposed. The procedure is described for elementary switch excitations. However, the same procedure is applicable to general switches as shown in Section II-E. It consists of the following nine steps.

*Step 1) Selecting the observation time (T):* This parameter is simply the time duration of interest and must be selected for each specific transient study.

*Step 2) Choosing the maximum allowed TD resolution ( $\Delta t_{\max}$ ):* This value does not directly affect the accuracy of the computations as MoM is solved in FD. Therefore, for optimized efficiency,  $\Delta t_{\max}$  should only be small enough to capture transients of interest (similar to the plot-step in EMT-type programs). As such, setting  $\Delta t_{\max}$  to values in the range of 250  $\mu\text{s}$  to 500  $\mu\text{s}$  is appropriate for many EMT applications. As seen in Step 6,  $\Delta t_{\max}$  has an indirect impact on the FD discretization and on the accuracy of computations, but this will be numerically verified in (9).

*Step 3) Computing the total number of time samples ( $N_t$ ):* This parameter should be an integer power of 2 for the FFTs to be efficient. It should also ensure a TD resolution  $\Delta t$  such that  $\Delta t \leq \Delta t_{\max}$ . Thus we have

$$N_t = 2^n, \quad n = \lceil \log_2(T/\Delta t_{\max}) \rceil \quad (6)$$

where  $\lceil \cdot \rceil$  denotes the ceiling function. Subsequently we have

$$\Delta t = T/(N_t - 1). \quad (7)$$

*Step 4) Obtaining the initial TD results:* The initial TD stage is required to compute the excitations in (2) or (5). Thus, depending on the case being a closer or an opener (1) or (4) is computed using  $T$  and  $\Delta t$ . This step requires a single MoM run as explained in Section II-B for a closer, and in Section II-C for an opener. Nevertheless, for reasons that will become clear in Step 9, the MoM cases from both sections are computed.

*Step 5) Obtaining the FD components:* Using (2) or (5), the FD components of the excitation are computed. As the excitation in TD has only real values, a total of  $N_f = (N_t/2)+1$  unique frequency samples are obtained where

$$f_{\min} = 0, \quad f_{\max} = N_t/(2T), \quad \Delta f = f_{\max}/(N_f - 1) \quad (8)$$

all in Hz.

*Step 6) Verifying  $\Delta t_{\max}$  and subsequent parameters:* Now that the FD components of the switch excitation are available, it is possible to verify the discretization parameters obtained in Steps 1 to 5. The total observation time  $T$  is user dependent. Hence the first parameter to be evaluated is  $\Delta t_{\max}$ . As explained earlier, the frequency spectrum of switch excitations based on (2) and (5) does not oscillate as the frequency increases. Thus, the following criteria is used to validate  $\Delta t_{\max}$

$$|V_{f_{\max}}|/|V_{\max}| = \varepsilon \quad \text{or} \quad |I_{f_{\max}}|/|I_{\max}| = \varepsilon. \quad (9)$$

If  $\varepsilon$  is small enough (e.g.  $\varepsilon < 5\%$ ), the truncation error in FD will be small and thus the discretization parameters are reliable. However if  $\varepsilon$  is not sufficiently small, one needs to go back to Step 2 and choose a smaller  $\Delta t_{\max}$  until a small enough  $\varepsilon$  is observed. As MoM results in Step 4 are unchanged, this process has negligible impact on the overall computation time.

*Step 7) Performing multiple MoM runs according to (8):* Once a small enough  $\varepsilon$  in (9) is observed, the MoM system should be solved for the  $N_f$  frequencies in (8). However, it is important to realize that the frequencies defined in (8), may or may not include the fundamental frequency (50, or 60 Hz) at which the network energization(s) should be computed. In

order to include these sources regardless of (8), the “superposition principle” suggests computing the contribution from such sources separately (Step 9) and adding the results to those coming from the excitation representing the switch at the frequencies defined in (8). That is, the excitation in (2) or (5) is applied to the switch location while the network source(s) are set to zero. In order to ensure accurate MoM results, the conductors in the model should be subdivided into smaller segments based on the wavelength  $\lambda$  such that the maximum segment length is in the range of  $\lambda/10$  to  $\lambda/6$  [4]. While this criterion can be used to optimize computation time at different frequencies, usually, the finest discretization based on the highest frequency is applied in the software [12]. This allows for using the same segmentation in the 3-D model at all frequencies. For a typical power system study, this has negligible impact on the overall runtime due to the availability of parallel computing in software [12] and multiple cores in typical hardware. Further, the linear behavior of the EFIE is used to completely eliminate the need for creating multiple 3-D models. That is, the magnitude of switch excitations is set to unity (i.e., 1 V or 1 A) and a single model is solved by MoM at all frequencies. This solution is sometimes referred to as “unmodulated” spectrum [12]. The magnitude of the excitation at different frequencies is incorporated by multiplying the unmodulated voltage or current with (2) or (5). This is sometimes called the “modulated” spectrum. By applying IFFT on the modulated solution, the TD signal is obtained.

*Step 8) Ensuring numerically-convergent TD results:* It is important to realize that while  $f_{max}$  in (8) can be reliably used in MoM computations based on (9),  $\Delta f$  in (8) may not necessarily ensure accurate EMT results. That is, the truncation of the integration domain in IFFT [11] beyond  $f_{max}$  will have negligible impact on the resulting TD signal. However,  $\Delta f$  may not necessarily be small enough for the IFFT to sufficiently sample the integration domain and may prevent it from producing accurate TD results. Therefore, in order to ensure numerically convergent TD results, the FD discretization is refined by halving  $\Delta f$  while keeping the same  $f_{max}$  in the next set of MoM runs. This is equivalent to setting the observation time to twice that of the one used in Step 1 (i.e.,  $2T$ ) while keeping the same  $\Delta t_{max}$  found in Step 6. The rest of the parameters are computed using (6), (7), and (8). Since  $\Delta f$  is exactly halved,  $N_f$  MoM solutions from Step 7 can be reused while the extra  $(N_f - 1)$  MoM computations need to be performed. Subsequently,  $2N_f - 1$  MoM solutions are used in IFFT to compute TD results from 0 to  $2T$ . If the maximum difference between the TD samples obtained in Steps 7 and 8 (from 0 to  $T$ ) is smaller than an acceptable tolerance (e.g.  $< 5\%$ ), the TD results are accepted and the most updated waveform is selected as the final solution. Otherwise, the process continues, until results exhibit numerical convergence. When comparing TD waveforms, the typical relative error may produce unrealistically large errors for samples with near-zero values. Thus, the following normalized max error is used

$$MaxErr = \max \left\{ \frac{|x_k - x'_k|}{\max\{|x|, |x'|\}} \right\}, \quad k = 1, \dots, N_t \quad (10)$$

where  $x$  and  $x'$  represent the vectors of TD samples under comparison. It is important to note that the suggested iterative process has a twofold impact on the accuracy. Not only it

improves the accuracy by adding more FD samples into the computations as explained above, but it also prevents the IFFT from erroneously constructing a non-periodic waveform from 0 to  $T$  by oversampling it beyond  $T$ . In fact, expansions up to  $8T$  have been suggested [15]. As exemplified in Section III, an accurate TD solution is typically achieved with a total of 257 to 1025 MoM computations for slow transients. **For faster transients, however, the number of required frequencies may grow. This is because fast transients can lead to the abrupt change of the surrounding electromagnetic fields. Therefore, the full-wave numerical modeling of such phenomena can become computationally more challenging as high-frequency components need to be considered while at the same time abrupt changes in the frequency response need to be captured (see for example Fig. 10). However, this does not have a paralyzing effect on the proposed method as it uses an iterative procedure to numerically converge to a TD solution. Evidently, depending on the severity of such effects, more iterations are needed leading to higher computational complexity. Nevertheless, as exemplified in Section III-B, the TD numerical convergence can indeed be achieved for very fast transients with a reasonable number of MoM runs (typically 2049 to 8193 simulations).**

*Step 9) Superimposing the TD results:* The contribution from the network source(s) are equivalent to the final TD stage defined in Fig. 2. For a closer, this can be computed by  $\sigma_1 \cdot i^0(t)$  and for an opener it is obtained by  $\sigma_1 \cdot v^0(t)$  where  $\sigma_1$ ,  $i^0$ , and  $v^0$  are defined in (3), (4), and (1), respectively. This is the reason for computing both MoM solutions in Step 4. The resulting TD signal is added to the computed TD signal in Step 8 to get the final (superimposed) TD solution.

### E. Modeling a general switch

In order to model a general switch (Fig. 1) (with arbitrary number of switch operations) using MoM, one needs to apply switch excitations in a sequential manner as depicted in Fig. 3.

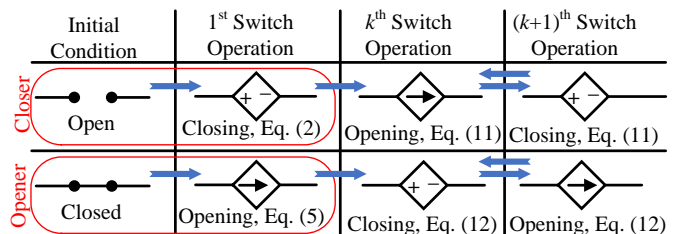


Fig. 3. Performing multiple switch operations based on the initial condition.

At each stage, a new switch excitation is included into the computations where the TD results at the end of each stage are obtained for the entire time (0 to  $T$ ) but with one extra switch operation compared to the previous stage. This is somewhat unintuitive as EMT results are expected to progress in time rather being updated for the entire time as subsequent switch maneuvers are incorporated. Nonetheless, this is a common practice when superposition principle is used to perform switch operations in FD methods [2].

If the initial condition is open, a closer is first used to close the switch as the 1<sup>st</sup> switch operation at  $t_s^1$ . As detailed in Section II-D, this computes transient parameters for the entire time duration  $T$  anywhere in the network assuming a single closing operation. The current flowing into the switch from

this first stage  $i^1(t)$  is saved and will be used in the next stage. In order to perform the 2<sup>nd</sup> switch operation (opening) at  $t_s^2$ , a current source is placed instead of the switch in the network with excitation  $I^2(f)$  that has its initial TD stage as  $i^1(t)$  but with the final TD stage of an opener in Fig. 2. Therefore, we have  $I^2(f) = FFT\{i^1(t) \cdot \sigma_2(t, t_s^2)\}$  where  $\sigma_2$  is defined in (3). Note that  $\sigma_1$  is not used, as the causality has already been enforced in the 1<sup>st</sup> stage. By applying the procedure in Section II-D on  $I^2(f)$ , the TD voltage signal across the switch  $v^2(t)$  is obtained for the entire time duration  $T$ , assuming both the 1<sup>st</sup> and 2<sup>nd</sup> switch operations at  $t_s^1$  and  $t_s^2$ , respectively. In order to perform the 3<sup>rd</sup> switch operation (closing) at  $t_s^3$ , the switch is replaced with a voltage source with the excitation  $V^3(f) = FFT\{v^2(t) \cdot \sigma_2(t, t_s^3)\}$  which can be used in the procedure of Section II-D to compute  $i^3(t)$  and simulate the next opening operation as was done in the 2<sup>nd</sup> switch operation. In general, if the initial condition of a switch is open, the MoM excitations after the 1<sup>st</sup> operation are

$$\begin{aligned} I^k(f) &= FFT\{i^{k-1}(t) \cdot \sigma_2(t, t_s^k)\}, \\ V^{k+1}(f) &= FFT\{v^k(t) \cdot \sigma_2(t, t_s^{k+1})\}, \quad k = 2, 4, 6, \dots \end{aligned} \quad (11)$$

At every stage, the applied excitation acts as a reminder that enforces all switch operations prior to that stage as well as the latest one. This is an important feature of the superposition principle because the latest MoM solution can be used in an IFFT to obtain the desired transient parameter (voltage, current, electric field, magnetic field, etc.) anywhere in the network when superimposed with its final TD stage. This eliminates the need for preserving results from earlier stages.

Similarly, for a general switch that is initially closed (see Fig. 3), an opener is used to simulate the 1<sup>st</sup> switch operation followed by the following excitations

$$\begin{aligned} V^k(f) &= FFT\{v^{k-1}(t) \cdot \sigma_2(t, t_s^k)\}, \\ I^{k+1}(f) &= FFT\{i^k(t) \cdot \sigma_2(t, t_s^{k+1})\}, \quad k = 2, 4, 6, \dots \end{aligned} \quad (12)$$

#### F. Modeling multiple general switches

The methodology used for a single general switch is applicable to multiple switches where the switch operations are still sequentially performed according to their operation time but may be applied at different locations. For example, if there are 2 switches at locations  $A$  and  $B$  in the network and they operate at  $t_A^1, t_A^2$  and  $t_B^1, t_B^2, t_B^3$  such that  $t_A^1 < t_B^1 < t_A^2 = t_B^2 < t_B^3$ , there will be a total of 4 stages. At stage 1, the switch operation is applied at location  $A$  while location  $B$  remains in its initial stage. At stage 2, the switch operation is applied at location  $B$  while location  $A$  has the excitation from its previous stage. At stage 3, both locations are updated according to their switch operations. Finally at stage 4, the switch operation is applied at location  $B$  while location  $A$  remains at its last stage. The final EMT results are obtained from the excitations at location  $A$  in stage 3, and the excitation at location  $B$  in stage 4.

#### G. The EFIE formulation

In the examples described in this paper, the commercial software CDEGS-MultiFields [12] is used to obtain full-wave 3-D MoM solutions. MultiFields provides a modified EFIE formulation that is capable of modeling energized networks

buried in or placed above a stratified lossy ground in the frequency range from 0 Hz to several GHz. The original and pioneering formulation which was developed by one of the authors in the mid-eighties [16], [17] does not suffer from the low-frequency breakdown as a consequence of the decoupling of the electric fields and magnetic fields at zero frequency. Consequently, it leads to a well-balanced and stable system from DC to the kHz range. In fact, the electromagnetic fields computations with this original low-frequency focus evolved to the MHz range [18]–[21], with present capability in the GHz range [22]. Field measurements in a complex substation environment demonstrated the low-frequency stability of the approach [23]. Detailed information on the derivations and related validations of the method are available in [16]–[31].

### III. RESULTS AND DISCUSSION

#### A. Pipe induced voltage due to aerial line fault

1) *Problem description:* In order to demonstrate the proposed methodology in the context of a typical power system study, we present results for a realistic situation where circuit theory and field theory models are used for cross-validation. As explained in Section I, the model based on circuit theory is created and the results are compared with the full-wave 3-D EMT results obtained from MoM using the proposed methodology. If matching results are observed, both models are verified as they are computed using fundamentally different approaches (i.e., circuit theory vs. field theory).

The problem is depicted in Fig. 4(a). A 20 km 3-phase overhead line is energized with a balanced 50 Hz source (230 kV RMS) with a 30  $\Omega$  load on the other end of the line. There is also an underground-coated pipe running parallel to the overhead line terminated with 0.1  $\Omega$  resistive grounding system on both sides. Note that more details and complexities such as 3-D grounding systems, observation points for electromagnetic fields (electric, magnetic, potential, current) anywhere in the 3-D space, non-parallel line and pipe, multilayer soil, etc., could have been considered in the 3-D full-wave model. However, they are not included to be consistent with the circuit-based model.

The goal is to predict the induced voltage on the metallic surface of the pipe if a fault occurs between the top and center conductors of the overhead line 10 km away from both sides. This is shown in Fig. 4(a) with the fault occurring between points  $A$  and  $B$ . The induced voltage is calculated at point  $P$  on the pipe. The fault starts at 0.03 s and lasts for 0.01 s. The same example is depicted in Fig. 4(b) based on the circuit notations used in the commercial EMT-type program, PSCAD/EMTDC [13]. While the transmission line parameters are computed separately for the TD circuit approach, they are obtained indirectly as an integral part of the 3-D EMT method.

This specific example has been selected as it may legitimately raise the following questions when circuit-based models are used. 1) The transmission line model is based on the TEM assumption which is valid for infinitely long lines. Is 10 km long enough for the  $T1$  and  $T2$  models in Fig. 4(b) to accurately represent the EMT phenomena occurring in this fault scenario? 2) The transmission line model is frequency

dependent. Can the frequency parameters ( $f_{\max}$ ,  $\Delta f$ ) used in  $T1$  and  $T2$  ensure accurate EMT results in this example? 3) The mutual couplings between the aerial conductors and the buried pipe have a direct impact on the induced voltage  $E_{\text{pipe}}$ . Can classical formulas such as the Lucca approximation [13] accurately compute the mutual couplings in this case?

Such uncertainties are addressed numerically by comparing the results to the full-wave computations.

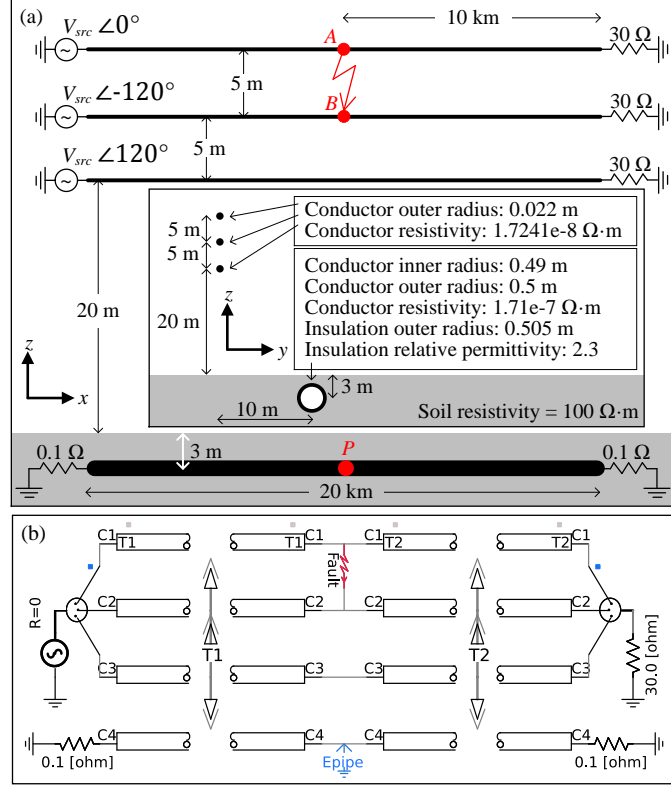


Fig. 4. (a) The problem depicted from an  $x$ - $z$  view. The inset is from a  $y$ - $z$  view showing line/pipe data. (b) Circuit-theory representation of the problem.

2) *Applying the proposed methodology*: As the fault is not present until 0.03 s, the initial condition for this problem is “open”. Thus, according to Section II-E, the fault is first applied at  $t_s^1 = 0.03$  s using a closer by following the steps in Section II-D as follows. Based on Steps 1 and 2,  $T = 0.1$  s and  $\Delta t_{\max} = 500 \mu\text{s}$  are chosen. Based on Step 3, we have  $n = 8$ ,  $N_i = 256$ , and  $\Delta t = 392.15 \mu\text{s}$ . According to Step 4, (1) should be computed where a ramp-up time  $t_r$  is required. We choose  $t_r = 1/f = 0.02$  s. The 3-D model in Fig. 4(a) is created using [12] with no connection (gap) between points A and B. The aerial conductors are energized with single-phase (peak) voltage  $V_{\text{src}} = \sqrt{2/3} \cdot 230$  kV and  $120^\circ$  apart. The MoM is run at 50 Hz and the potential at points A and B are computed to be  $180.623 \angle -6.6^\circ$  and  $183.282 \angle -126^\circ$  kV, respectively. Hence, we have  $A_v = 314.196$  kV and  $\phi_v = 23.94^\circ$  which can be used to compute the initial TD stage  $v^0(t)$  using (1) as plotted in Fig. 5.

Next, the MoM is run with identical parameters, but with a low resistivity conductor (e.g. copper) placed between points A and B. Subsequently, we get  $A_i = 45.631$  kA and  $\phi_i = -57.2^\circ$  which will be used in Step 9. According to Step 5, the FD components of the first switch excitation  $V^1$  are obtained using (2), which is plotted in Fig. 5 in terms of its magnitude  $|V^1|$ .

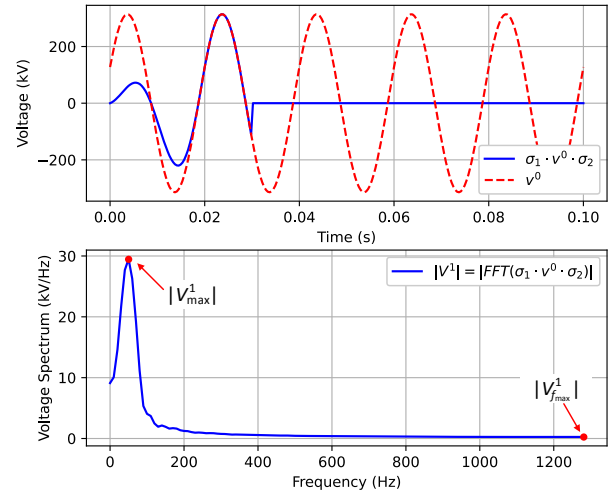


Fig. 5. TD signal for closing operation (applying fault) and its FD spectrum.

According to (8), it has  $N_f = 129$  unique frequency samples with  $f_{\min} = 0$  Hz,  $f_{\max} = 1280$  Hz and  $\Delta f = 10$  Hz. The criteria in (9) is  $\epsilon = 0.25$  kV/29.5 kV = 0.84% which is considered small enough for the discretization parameters to be reliable for this excitation. This allows us to move on to Step 7 and run MoM at all 129 frequencies where the network energizations are set to zero in Fig. 4(a) (i.e.,  $V_{\text{src}} = 0$  V), but a unit voltage source ( $V = 1 \angle 0^\circ$  V) is placed between points A and B. The resulting unmodulated solution is multiplied by  $V^1$  to get the modulated spectrum and subsequently transformed into TD using IFFT. This is shown in Fig. 6 as iteration 1. It is clear that this TD signal violates causality. Hence, as suggested in Step 8, the TD discretization is refined by doubling the time duration until a numerically convergent TD signal is observed. Results are plotted in Fig. 6 all from 0 to  $T$  for better clarity. The maximum difference between the  $4T$  and  $8T$  plots based on (10) is about 2.24%. Hence, the stopping criteria has been met and the TD samples from the 4<sup>th</sup> iteration are selected as the final solution for Step 8. Note that in addition to the 129 MoM runs performed in Step 7 (iter1), an additional 128, 256, and 512 MoM computations are done for the 2<sup>nd</sup>, 3<sup>rd</sup>, and 4<sup>th</sup> iterations, respectively. Therefore, 1025 MoM runs have produced all plots shown in Fig. 6. It is worth noting that a mere DC shift would not correct the  $1T$  and  $2T$  plots for all time samples, making such an iterative process essential.

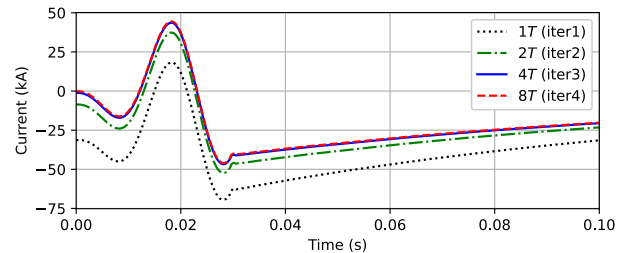


Fig. 6. Illustration of TD numerical convergence proposed in Section II-D8.

Using  $A_i = 45.631$  kA and  $\phi_i = -57.2^\circ$  computed in Step 4, the final TD stage  $\sigma_1 \cdot i^0(t)$  is computed and added to the 4<sup>th</sup> iteration results. This is plotted as  $i^1$  in Fig. 7 which is essentially the fault current if the fault occurs from 0.03 s and not cleared. In order to clear the fault at  $t_s^2 = 0.04$  s, the excitation in (11) is computed as shown in the bottom graph of Fig. 7 and used in the procedure of Section II-D.

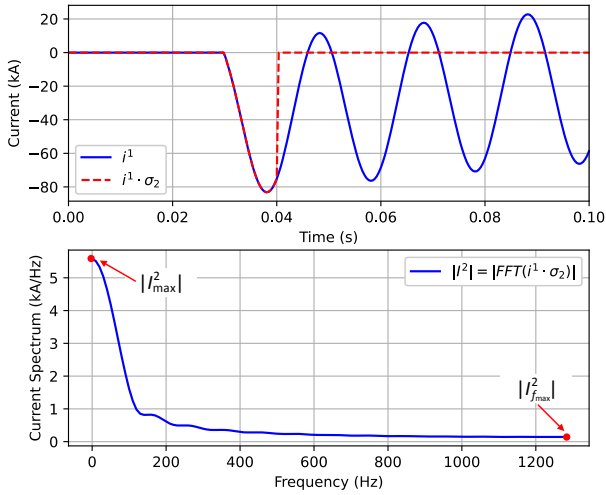


Fig. 7. TD signal for opening operation (clearing fault) and its FD spectrum.

The discretization parameters for  $T = 0.1$  s and  $\Delta t_{\max} = 500$   $\mu$ s are such that  $\epsilon$  in (9) is  $0.14$  kA/5.57 kA = 2.59%. This requires 129 MoM runs where the network energizations are set to zero in Fig. 4(a) (i.e.,  $V_{src} = 0$  V), but a unit current source ( $I = 1 \angle 0^\circ$  A) is placed between points *A* and *B*. In order to achieve numerical convergence at Step 8, we monitor the induced voltage on the pipe directly as there will be no more switch operations in this example. It is found that numerically convergent TD results are achieved with 2 iterations, with a maximum error (10) of about 1.29%. Therefore, 257 MoM computations are sufficient for clearing the fault. By adding the (small) contribution from the final TD stage with the results obtained from the 2<sup>nd</sup> iteration, the induced voltage on the pipe is computed and plotted in Fig. 8. Comparisons with the results produced by the EMT-type program [13] confirm that not only the proposed methodology has correctly predicted the induced voltage on the pipe, it is also a numerical validation of the assumptions made in the circuit-based model discussed earlier.

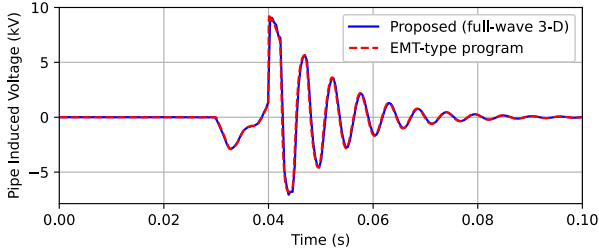


Fig. 8. Voltage induced on the pipe computed using different techniques.

### B. Very fast transients in gas-insulated substations

1) *Problem description:* In order to demonstrate the applicability of the proposed method to EMT analysis with high-frequency phenomena, we study very fast transients that are known to occur in gas-insulated substations (GIS) [7]. Again, in order to be consistent with the circuit-based model of the EMT-type program, a simple gas-insulated bus (GIB) is considered as depicted in Fig. 9. The GIB is energized by closing the switch at  $0.1$   $\mu$ s and the voltage on the open end of the GIB ( $V_{core}$ ) is monitored.

2) *Applying the proposed methodology:* The methodology is applied as explained before, except that the final TD stage also requires multiple MoM runs. This is because despite the

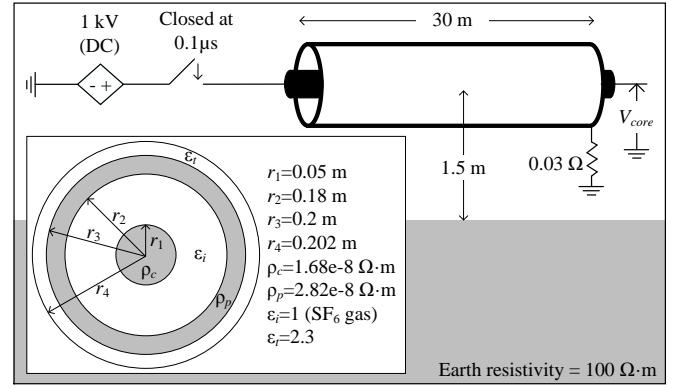


Fig. 9. Model of a gas-insulated bus (GIB).

excitation being DC, the rise time (before  $t_r$ ) and fall time (beyond  $T$ ) will produce higher frequency components. Thus, the iterative process explained in Section II-D8 is carried out to find the appropriate frequency domain discretization when computing the final TD stage. Note that in the procedure, we set  $T = 5$   $\mu$ s and  $\Delta t_{\max} = 0.01$   $\mu$ s. Therefore, we have  $f_{\max} = 50.7$  MHz and  $\Delta t = 0.0098$   $\mu$ s. Subsequently, the numerical convergence is achieved after 4 iterations by solving the MoM system at a total of 2049 frequencies with  $\Delta f = 24.75$  kHz. Results are plotted in Fig. 10.

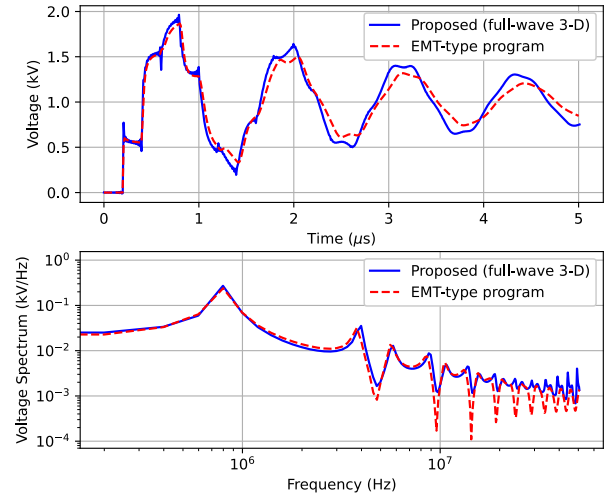


Fig. 10. Core voltage at the open-circuit end. FD results (bottom graph) are obtained by taking the FFT of the TD results (top graph) for both methods.

It can be seen that the EMT-type program [13] and the proposed methodology have produced similar results in terms of the transient waveform with a dominant frequency of about 800 kHz. However, the high-frequency oscillating components observed in the full-wave approach are not present in the results produced by the EMT-type program. This is consistent with the findings in [7], where it was shown that high-frequency components (greater than 10 MHz) in the step response of a GIB lead to a “spike-like” behavior at the voltage wave-front in TD due to the transition effects from the TEM mode at low frequencies to high frequency Sommerfeld–Goubau (surface wave) propagation mode [32]. In the TD results of Fig. 10 such effects are visible in the full-wave results, especially before 2  $\mu$ s. But such spikes are not seen in the results produced by the EMT-type program. This can also be seen in the FD results of Fig. 10 where the two plots well-agree at lower frequencies up to about 3 MHz, but they start to deviate at higher frequencies.

#### IV. CONCLUSIONS

A methodology for performing full-wave 3-D EMT analysis of switch operations and faults is introduced. It is based on the application of superposition principle on MoM solution of the EFIE. It is demonstrated that such solutions can be used to perform practical and realistic transient studies. This method can be used to calibrate and validate modelling assumptions in conventional EMT-type programs when measurement results are not available. For example, it is shown that for slow transients, the full-wave and conventional EMT simulations produce well-matching results. However, in applications with fast transients, the full-wave approach can provide more realistic simulation results. In order to remain consistent with the models of the EMT-type programs, the “geometrical” 3-D aspects of the proposed methodology was not demonstrated (e.g. a 3-D model of a GIS) and parameters important in studies involving electromagnetic compatibility and interference were not studied. Such capabilities of the proposed technique will be investigated in future studies. Furthermore, the method will be extended to include frequency-dependent multilayer soil parameters and nonlinear devices such as metal oxide surge arresters and power transformers. Inclusion of logarithmic scale FD discretization and the use of the NLT will also be explored.

#### REFERENCES

- [1] A. Ametani, "Electromagnetic Transients Program: History and Future," *IEEE Trans. Elec. Electron. Eng.*, 2020.
- [2] P. Moreno and A. Ramirez, "Implementation of the Numerical Laplace Transform: A Review," *IEEE Trans. Power Del.*, vol. 23, no. 4, pp. 2599-2609, Oct. 2008.
- [3] A. Tatematsu, S. Moriguchi and T. Ueda, "Switching Surge Analysis of an EHV Air-Insulated Substation Using the 3-D FDTD Method," *IEEE Trans. Power Del.*, vol. 33, no. 5, pp. 2324-2334, Oct. 2018.
- [4] M. Nazari, R. Moini, S. Fortin, F. P. Dawalibi and F. Rachidi, "Impact of Frequency-Dependent Soil Models on Grounding System Performance for Direct and Indirect Lightning Strikes," *IEEE Trans. Electromagn. Compat.*, doi: 10.1109/TEMC.2020.2986646.
- [5] CIGRE Working Group C4.501, "Guideline for numerical electromagnetic analysis method and its application to surge phenomena," *CIGRE Tech. Brochure*, vol. 543, Jun. 2013.
- [6] M. Shafieipour, Z. Chen, A. Menshov, J. De Silva, V. Okhmatovski, "Efficiently computing the electrical parameters of cables with arbitrary cross-sections using the method-of-moments," *Electric Power Systems Research*, vol. 162, pp. 37-49, 2018.
- [7] H. Xue, A. Ametani, J. Mahseredjian, Y. Baba, F. Rachidi and I. Kocar, "Transient Responses of Overhead Cables Due to Mode Transition in High Frequencies," *IEEE Trans. Electromagn. Compat.*, vol. 60, no. 3, pp. 785-794, Jun. 2018.
- [8] L.M Wedepohl, D.J. Wilcox, "Transient Analysis of Underground Power Transmission Systems," *Proc. IEE*, vol. 120, no. 2, pp. 253-260, Feb. 1973.
- [9] S. Mohammadi, H. Karami, M. Azadifar, M. Rubinstein and F. Rachidi, "Assessing the Efficacy of a GPU-Based MW-FDTD Method for Calculating Lightning Electromagnetic Fields Over Large-Scale Terrains," *IEEE Let. Electromag. Compat. Pract. App.*, vol. 2, no. 4, pp. 106-110, Dec. 2020.
- [10] B. Salarieh, J. De Silva, A. M. Gole, A. Ametani and B. Kordi, "An Electromagnetic Model for the Calculation of Tower Surge Impedance Based on Thin Wire Approximation," *IEEE Trans. Power Del.*, doi: 10.1109/TPWRD.2020.3003250.
- [11] J. de Jesus Chavez, A. Ramirez, V. Dinavahi, R. Iravani, J. A. Martinez, J. Jatskevich and G. W. Chang, "Interfacing Techniques for Time-Domain and Frequency-Domain Simulation Methods," *IEEE Trans. Power Del.*, vol. 25, no. 3, pp. 1796-1807, July 2010.
- [12] "CDEGS 16.0.7172," Safe Engineering Services & technologies Ltd., [Online]. Available: <https://www.sestech.com/>. [Accessed 16 Oct. 2020].
- [13] "PSCAD/EMTDC manual," Manitoba Hydro International Ltd., [Online]. Available: <https://hvdc.ca/pscad/>. [Accessed 16 Oct. 2020].
- [14] A. Ametani and K. Imanishi, "Development of exponential Fourier transform and its application to electrical transients," *Proc. IEE*, vol. 126, no. 1, pp. 51-56, 1979.
- [15] Peter V. O'Neil, *Advanced Engineering Mathematics*, 7 ed., Thomson-Engineering, 2011, p. 497.
- [16] F. P. Dawalibi, "Electromagnetic Fields Generated by Overhead and Buried Short Conductors Part 1 - Single Conductor," *IEEE Trans. Power Del.*, vol. 1, no. 4, pp. 105-111, Oct. 1986.
- [17] F. P. Dawalibi, "Electromagnetic Fields Generated by Overhead and Buried Short Conductors Part 2 - Ground Networks," *IEEE Trans. Power Del.*, vol. 1, no. 4, pp. 112-119, Oct. 1986.
- [18] L. Grcev and F. P. Dawalibi, "An electromagnetic model for transients in grounding systems," *IEEE Trans. Power Del.*, vol. 5, no. 4, pp. 1773-1781, Oct. 1990.
- [19] F. P. Dawalibi, "Computation of electromagnetic fields produced by electric power lines and residential electrical wiring," *IEEE Trans. Power Del.*, vol. 8, no. 3, pp. 1285-1294, July 1993.
- [20] F. P. Dawalibi and A. Selby, "Electromagnetic fields of energized conductors," *IEEE Trans. Power Del.*, vol. 8, no. 3, pp. 1275-1284, 1993.
- [21] A. Selby and F. Dawalibi, "Determination of current distribution in energized conductors for the computation of electromagnetic fields," *IEEE Trans. Power Del.*, vol. 9, no. 2, pp. 1069-1078, Apr. 1994.
- [22] M. Nazari, R. Moini, S. Fortin and F. P. Dawalibi, "On the Performance of Grounding, Bonding, and Shielding Systems for Direct and Indirect Lightning Strikes," *IEEE Trans. Electromagn. Compat.*, vol. 62, no. 1, pp. 135-143, Feb. 2020.
- [23] W. K. Daily and F. Dawalibi, "Measurements and computations of electromagnetic fields in electric power substations," *IEEE Trans. Power Del.*, vol. 9, no. 1, pp. 324-333, Jan. 1994.
- [24] W. Xiong and F. P. Dawalibi, "Transient performance of substation grounding systems subjected to lightning and similar surge currents," *IEEE Trans. Power Del.*, vol. 9, no. 3, pp. 1412-1420, July 1994.
- [25] F. P. Dawalibi, W. Ruan, and S. Fortin, "Lightning Transient Response of Communication Towers and Associated Grounding Networks," in *Proc. Inter. Conf. Electromagnet. Compat., ICEMC'95KUL*, Kuala Lumpur, Malaysia, Apr. 11-13, 1995.
- [26] F. P. Dawalibi, Wei Xiong and Jinxi Ma, "Transient performance of substation structures and associated grounding systems," *IEEE Trans. Ind. App.*, vol. 31, no. 3, pp. 520-527, May-June 1995.
- [27] H. Lee, F. P. Dawalibi, W. Ruan, and S. Fortin, "Performance of Gas-Insulated Substations and Associated Grounding Networks during Fault and Transient Conditions," in *Proc. 58th Ann. Meet. American Power Conf.*, Chicago, Apr. 9-11, 1996.
- [28] W. Ruan, S. Fortin, F. P. Dawalibi, and J. Ma, "Computation of Electromagnetic Fields Inside Buildings Located Close to High-Voltage Power Line," in *Proc. 58th Ann. Meet. American Power Conf.*, Chicago, April 9-11, 1996.
- [29] S. Fortin, F. P. Dawalibi, and J. Ma, "Computation of Induced Voltages on Electric Distribution Lines Due to an Indirect Lightning Strike," in *Proc. 13th Inter. Wroclaw Symp. Exhibit. Electromagnet. Compat.*, Wroclaw, Poland, June 25-28, 1996.
- [30] J. Ma, F. P. Dawalibi, and W. Ruan, "Analysis and Computation of Induced Voltages on Communication Cables Due to a Lightning Strike on a Parallel Transmission Line," in *Proc. 13th Inter. Wroclaw Symp. Exhibit. Electromagnet. Compat.*, Wroclaw, Poland, June 25-28, 1996.
- [31] F. P. Dawalibi, S. Fortin, W. Ruan, J. Ma, and S. G. Lodwig, "Analysis of Electric Transients during Capacitor Switching Operations in a Substation," in *Proc. 58th Ann. Meet. American Power Conf.*, Chicago, April 1-3, 1997.
- [32] J. Chiba, "Studies in overhead wire-Goubau line above ground," *IEEE Trans. Microw. Theory Tech.*, vol. 25, no. 2, p. 83-93, Feb. 1977.